PAPER

Check for updates

In silico screening of photostabilizing reagents for cyanine-based single molecule fluorescence†

Jorge E. Ramos-Sanchez, ‡§[a] Yasser Gidi, ‡¶[a] Terri C. Lovell,§[a] Liam Payne,‖[a] Aya Sakaya [ab] and Gonzalo Cosa ★[a]

Fluorophore signal and photostability are desirable when conducting single molecule fluorescence (SMF) studies. For cyanine dyes, this is typically achieved by quenching their excited triplet states *via* photoinduced electron transfer (P*e*T). However, to date, only a handful of electron donors or acceptors have been – empirically – identified, most of which do not show diffusion controlled P*e*T quenching rate constants (k_{PeT}). Here we report a screening tool to rapidly explore the potential of thiol-based electron donors to serve as photostabilizers of Cy3, Cy5, and their bridged congeners Cy3B and Cy5B. Based on density functional theory (DFT) and utilizing Marcus theory of electron transfer, our method estimates *in silico* the activation free energy of P*e*T. A correlation function is then established between theoretical estimates and empirical values of k_{PeT} acquired through transient absorption spectroscopy. The correlation function then enables screening of the photostabilizing potential of untested reagents from a kinetic standpoint. A new compound, glyceryl monothioglycolate (GMTG), was thus identified. SMF studies show the effectiveness of GMTG as a domestic use, non-toxic, non-volatile alternative to the widely utilized β-mercaptoethanol. Altogether, a predictive model is proposed toward discovering photostabilizers to achieve single molecule fluorescence experiments with enhanced photo- and signal stability.

[a] *Department of Chemistry and Quebec Center for Advanced Materials (QCAM), McGill University, 801 Sherbrooke Street West, Montreal, QC H3A 0B8, Canada. E-mail: gonzalo.cosa@mcgill.ca*

[b] *Department of Chemistry, University of Toronto, Toronto, ON M5S 3H6, Canada*

† Electronic supplementary information (ESI) available. See DOI: https://doi.org/10.1039/d4cp04794j
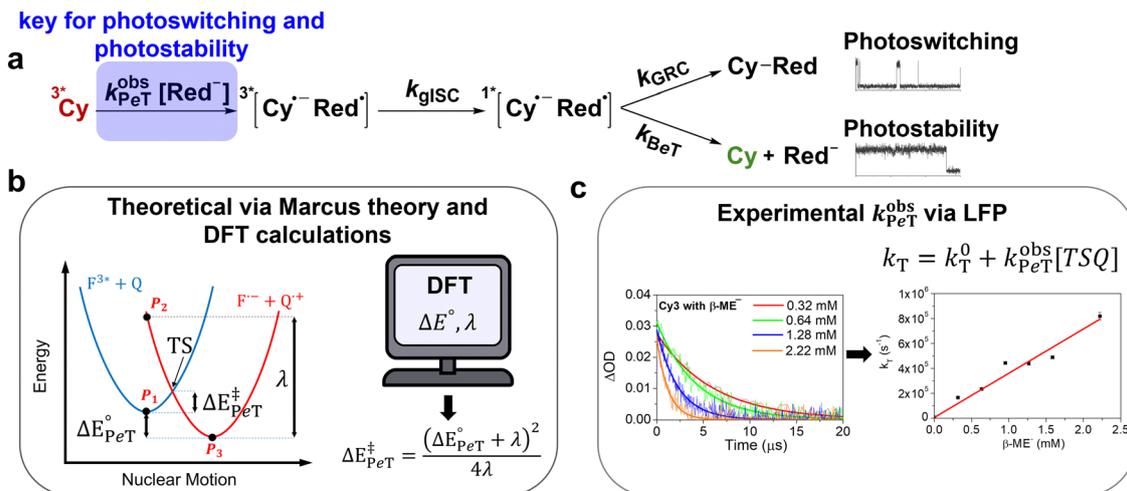
‡ These authors contributed equally.

§ Department of Chemistry and Biomolecular Science, University of Ottawa, Ottawa, ON K1N 6N5, Canada.

¶ Department of Radiology, School of medicine, Stanford University, Stanford, California 94305, United States.

‖ Discipline of Internal Medicine, Faculty of Medicine, Memorial University of Newfoundland, St. John's, NL A1B 3V6, Canada.

Introduction

Single molecule fluorescence (SMF) and single molecule localization microscopy (SMLM) techniques require high excitation energies to achieve high emission rates and thus maximize the signal-to-background ratio.[1–4] Here, it is critical to control the fate of the excited triplet state of fluorophores, which must be rapidly quenched/scavenged if and when formed.[5,6]

Quenching of the excited triplet state enhances the signal intensity and typically prevents photodamage, resulting in increased photostabilities in SMF. Triplet state quenching may also yield a desired photoproduct, *e.g.* a non-absorbing adduct that can be subsequently photo-uncaged, of interest in SMLM (Fig. 1a).[7–9] Carefully tuning the lifetime of the excited triplet state of the fluorophore has been instrumental to the many advances brought about by SMF and SMLM in biology, chemistry, physics, and materials science.[10–13]

Photoinduced electron transfer (P*e*T) has become the method of choice to quench fluorophores in their excited triplet state.[13,14] Water soluble electron donors can be utilized at concentrations high enough to quench excited triplet states, while sparing the excited singlet state.[15] While typically a counter oxidant may be needed in conjunction with the electron donor, when using thiol-based electron donors, such counter oxidants are not required. This is because newly formed thiyl radicals undergo rapid spin flip enabling back electron transfer (B*e*T) to occur in a spin allowed process within the solvent cage, before escape of newly formed radicals takes place (Fig. 1a).[16–18] Notably, while the chemical space offers limitless possibilities for thiol-based electron donors, only a handful of these types of reagents have been identified to date. This is largely explained by the fact that the screening of these compounds is a highly laborious task, requiring bulk time resolved studies to determine the rate constants of P*e*T and single molecule studies to then validate the performance of such compounds.

To accelerate the discovery of novel and improved triplet state quenchers, here we report a density functional theory (DFT)-based method to estimate P*e*T activation energy ($\Delta E^{\ddagger}_{PeT}$) and rate constant ($k_{PeT}$) values for the quenching of the excited

This journal is © the Owner Societies 2025

Phys. Chem. Chem. Phys., 2025, **27**, 9227–9234 | **9227**

Fig. 1 Triplet state quenching as a photocontrol strategy and parameters measured in this study. (a) Reaction scheme illustrating the excited triplet state in cyanine dyes and its downstream pathways after excited triplet state quenching associated with photostability or photoswitching. (b) Theoretical activation energies were calculated *via* DFT modelling. The blue parabola represents a cyanine in the triplet excited state (F^{3*}) and a triplet state quencher (Q) in the ground state. P_1 represents the reactant coordinate in the optimized structure. The red parabola represents the products of the reaction, namely the one electron reduced fluorophores and the one electron oxidized electron donor. P_3 represents the product coordinate in its optimized structures, while P_2 corresponds to the product coordinate in the reactant geometry (vertical transition). (c) Experimental P*e*T rate constants ($k_{\text{P}e\text{T}}^{\text{obs}}$) obtained by fitting the excited triplet state decay obtained *via* LFP at various TSQ concentrations.

triplet state of the single-molecule fluorophores Cy3, Cy5 and their bridged congeners Cy3B and Cy5B.[19] Our method relies on obtaining *via* DFT – utilizing Marcus theory of electron transfer – the parameters to calculate the activation energy ($\Delta E_{\text{P}e\text{T}}^{\ddagger}$, Fig. 1b), namely the electronic energy change ($\Delta E_{\text{P}e\text{T}}^{\circ}$) and the reorganization energy (λ) of P*e*T. We next correlate the theoretically estimated values of $\Delta E_{\text{P}e\text{T}}^{\ddagger}$ with empirical values for the P*e*T rate constant ($k_{\text{P}e\text{T}}^{\text{obs}}$) obtained through bulk laser flash photolysis (LFP) studies (Fig. 1c). The correlation then enabled us to utilize predicted activation energy parameters to estimate rate constants of P*e*T for unknown compounds. In our work, we utilized popular electron donating triplet state quenchers (TSQs): β-mercaptoethanol (β-ME),[16,20] ascorbic acid (AA),[21] *n*-propyl gallate (*n*-PG),[15,22] and the vitamin E analogue Trolox (TX)[11,23,24] in combination with four cyanine dyes (Cy3, Cy3B, Cy5 and Cy5B; Table 1).

The excellent correlation between empirical $k_{\text{P}e\text{T}}^{\text{obs}}$ values and theoretical $\Delta E_{\text{P}e\text{T}}^{\ddagger}$ values (while not $\Delta G_{\text{P}e\text{T}}^{\circ}$) positions our predictive model as a suitable tool to rapidly evaluate the potential of existing and newly designed compounds to serve as photostabilizers of cyanine dyes. As a case example, our method screened a range of compounds, primarily based on the values of $k_{\text{P}e\text{T}}^{\text{obs}}$, but also introducing solubility and pK_a as additional selection parameters. Improved photostability is predicted and shown with GMTG, a low vapor pressure alkyl thiol-based compound – of ample use in the cosmetic industry for perms[26] – that surpasses the performance of β-ME, providing an odorless, inexpensive, and safe-to-operate P*e*T-based photostability and photoswitching agent.

The predictive model proposed to select photostabilizers, while centered on cyanine dyes, should be of general applicability to other fluorophores utilized in SMF experiments, toward conducting experiments with enhanced photo- and signal stability.

Results and discussion

DFT modelling of P*e*T activation energy using Marcus theory of electron transfer

To estimate the activation energy values of P*e*T ($\Delta E_{\text{P}e\text{T}}^{\ddagger}$, eqn (1)), we utilized Marcus theory of electron transfer relating the activation energy, the electronic energy change for P*e*T ($\Delta E_{\text{P}e\text{T}}^{\circ}$), and the reorganization energy (λ).[27] We note that, for all calculations, we used electronic energy changes ($\Delta E_{\text{P}e\text{T}}^{\circ}$) instead of Gibbs free energy changes ($\Delta G_{\text{P}e\text{T}}^{\circ}$) because λ values need to be calculated from geometries outside their energetic minima, which precludes from performing accurate frequency calculations and associated thermodynamic values.[28]

$$\Delta E_{\text{P}e\text{T}}^{\ddagger} = \frac{\left(\Delta E_{\text{P}e\text{T}}^{\circ} + \lambda\right)^2}{4\lambda} \qquad (1)$$

To obtain $\Delta E_{\text{P}e\text{T}}^{\circ}$ and λ, we next performed DFT calculations using the B3LYP functional with the polarizable continuum model (PCM, water) for solvation. Here, we parameterized the reactants separately using the Gaussian package v.16,[29] as previously described by Buda[30] (see Section S1.2, ESI,† for more information). We first optimized the cyanines in the excited triplet state at their minimum (Fig. 1b, P_1) using time dependent DFT (TD-DFT). We "froze" the molecule with the solvent charges using the "NONEQ" keyword formalism in Gaussian and added an electron to the cyanine to perform a vertical transition (Fig. 1b, P_2). The molecular geometry was then optimized to accommodate for the new electron (Fig. 1b, P_3).

Table 1 Measured photoinduced electron transfer rate constants (k_{PeT}^{obs}, M^{-1} s^{-1}), calculated free energy (ΔE_{PeT}°, eV) and activation energy ($\Delta E_{PeT}^{\ddagger}$, eV) for all TSQ–cyanine combinations

		Cy3	Cy3B	Cy5	Cy5B
β-ME	k_{PeT}^{obs}	$3.54 \pm 0.23 \times 10^8$	$1.94 \pm 0.18 \times 10^7$	$9.44 \pm 0.43 \times 10^7$	$1.30 \pm 0.39 \times 10^6$
	ΔE_{PeT}°	−0.46	−0.11	−0.22	0.04
	$\Delta E_{PeT}^{\ddagger}$	0.40	0.55	0.49	0.60
AA	k_{PeT}^{obs}	$4.41 \pm 0.14 \times 10^8$	$6.93 \pm 0.23 \times 10^7$	$2.54 \pm 0.16 \times 10^8$	$1.19 \pm 0.06 \times 10^7$
	ΔE_{PeT}°	−0.51	−0.16	−0.27	−0.004
	$\Delta E_{PeT}^{\ddagger}$	0.35	0.50	0.45	0.55
TX	k_{PeT}^{obs}	$1.17 \pm 0.04 \times 10^9$	$2.91 \pm 0.97 \times 10^8$	$1.19 \pm 0.12 \times 10^8$	$5.49 \pm 2.19 \times 10^7$
	ΔE_{PeT}°	−0.42	−0.07	−0.18	0.08
	$\Delta E_{PeT}^{\ddagger}$	0.32	0.47	0.41	0.52
n-PG	k_{PeT}^{obs}	$7.64 \pm 0.65 \times 10^8$	$1.14 \pm 0.06 \times 10^9$	$8.07 \pm 0.72 \times 10^8$	$5.99 \pm 1.00 \times 10^8$
	ΔE_{PeT}°	−0.82	−0.47	−0.58	−0.32
	$\Delta E_{PeT}^{\ddagger}$	0.18	0.30	0.26	0.34
2-TH	$^a k_{PeT}^{obs}$	$1.37 \pm 0.13 \times 10^9$	$5.42 \pm 0.16 \times 10^8$	$9.15 \pm 0.30 \times 10^8$	$1.22 \pm 0.04 \times 10^8$
	ΔE_{PeT}°	−0.55	−0.20	−0.31	−0.05
	$\Delta E_{PeT}^{\ddagger}$	0.30	0.44	0.39	0.49
Erg	$^a k_{PeT}^{obs}$	$3.77 \pm 0.77 \times 10^8$	$7.78 \pm 0.27 \times 10^8$	$1.11 \pm 0.06 \times 10^9$	$3.52 \pm 0.21 \times 10^8$
	ΔE_{PeT}°	−0.93	−0.33	−0.44	−0.18
	$\Delta E_{PeT}^{\ddagger}$	0.15	0.38	0.33	0.42
GMTG	k_{PeT}^{obs}	$2.35 \pm 0.08 \times 10^8$	$1.73 \pm 0.12 \times 10^6$	$2.19 \pm 0.10 \times 10^7$	$^b 1.61 \pm 0.43 \times 10^5$
	ΔE_{PeT}°	−0.33	0.02	−0.09	0.15
	$\Delta E_{PeT}^{\ddagger}$	0.44	0.60	0.54	0.65

^{a} Values taken from ref. 25. ^{b} Determined with only 3 points.

A similar treatment was performed on the TSQ, where the ground state was optimized (Fig. 1b, P_1), an electron was removed from the molecule (Fig. 1b, P_2) and then it was optimized to accommodate for the loss of the electron (Fig. 1b, P_3). Energies were calculated from the three different points for each cyanine and TSQ independently (see Tables S1 and S2, ESI,† for values). ΔE_{PeT}° was obtained from the optimized structures (eqn (2)) for each donor–acceptor pair, while reorganization energies (λ) were calculated from the vertical excitations and the optimized product (eqn (3)). Finally, the activation energy $\Delta E_{PeT}^{\ddagger}$ for each combination was obtained according to eqn (4) where both free energy and reorganization energy were combined from both the fluorophore and the quencher. Results are summarized for each dye–TSQ combination in Table 1.

$$\Delta E_{PeT}^{\circ} = P_3 - P_1 \tag{2}$$

$$\lambda = P_3 - P_2 \tag{3}$$

$$\Delta E_{PeT}^{\ddagger} = \frac{\left(\left(\Delta E_F^{\circ} + \Delta E_Q^{\circ}\right) + \left(\lambda_F + \lambda_Q\right)\right)^2}{4\left(\lambda_F + \lambda_Q\right)} \tag{4}$$

Empirical k_{PeT} from transient absorption laser flash photolysis
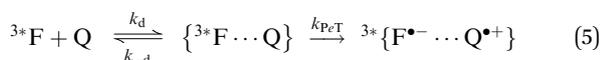
To obtain k_{PeT}^{obs}, the excited triplet state absorption of each dye was recorded over time in the presence of increasing TSQ concentrations utilizing an LFP (see Sections S1.3 and S1.4, ESI†). Four widely used and commercially available triplet state quenchers were measured: AA, β-ME, n-PG and TX (see Table 1). The chromophores were irradiated with the 10 ns, 10 mJ per pulse, 532 nm output of a Nd:YAG laser in the presence of 50 mM KI to promote intersystem crossing (ISC).[31,32] To avoid competition from dissolved oxygen, an enzymatic oxygen scavenger based on the glucose/glucose oxidase/catalase (GOD-CAT) system was used.[33] Plotting the obtained pseudo-first order decay rate constants as a function of TSQ concentration

yielded the values of $k_{\mathrm{P}e\mathrm{T}}^{\mathrm{obs}}$ and k_{T}^{0} (the excited triplet state decay rate constant in the absence of the quencher) from the slope and intercept of the plots, respectively (see Fig. 1c and Table 1 for data and Fig. S1–S4, ESI,† for graphs). In all cases, we used the concentration of the electron donor in its deprotonated form, calculated using their reported pK_a and the Henderson–Hasselbalch equation.

$\Delta E_{\mathrm{P}e\mathrm{T}}^{\ddagger}$ estimates and empirical $k_{\mathrm{P}e\mathrm{T}}^{\mathrm{obs}}$ correlation

To correlate the theoretically obtained $\Delta E_{\mathrm{P}e\mathrm{T}}^{\ddagger}$ with the $k_{\mathrm{P}e\mathrm{T}}^{\mathrm{obs}}$, we considered the reaction mechanism proposed in eqn (5). Here the electron acceptor (fluorophore, F) and the electron donor (quencher, Q) must be in close contact, inside the solvent cage, for PeT to occur. The overall reaction can then be modeled as taking place through three elementary steps, where the complex is formed with a rate constant k_{d} (the diffusion-controlled association rate constant) and it is depleted as the competition between complex dissociation ($k_{-\mathrm{d}}$) and $k_{\mathrm{P}e\mathrm{T}}$ (eqn (5)). Applying steady state conditions, $k_{\mathrm{P}e\mathrm{T}}^{\mathrm{obs}}$ is thus shown to arise from a combination of the above rate constants (see eqn (6), and Section S1.5, ESI,† for derivation). Utilizing the Eyring–Polanyi relationship between $k_{\mathrm{P}e\mathrm{T}}$ and the transition state energy (eqn (7)),[27] and replacing the value of $k_{\mathrm{P}e\mathrm{T}}$ in eqn (7), yields the mathematical relationship between $k_{\mathrm{P}e\mathrm{T}}^{\mathrm{obs}}$ and $\Delta E_{\mathrm{P}e\mathrm{T}}^{\ddagger}$ (eqn (8)). $\kappa(r)$ denotes the average transition probability for electron transfer to happen and υ is the collision frequency of the reactants. We note that this follows a formalism similar to that used by Rehm and Weller in correlating experimental $\Delta G_{\mathrm{P}e\mathrm{T}}^{\circ}$ with $k_{\mathrm{P}e\mathrm{T}}^{\mathrm{obs}}$ to learn on $k_{\mathrm{P}e\mathrm{T}}$.[34] Here, however, we correlated the theoretical predictions of $\Delta E_{\mathrm{P}e\mathrm{T}}^{\ddagger}$, rather than redox potentials obtained from electrochemical measurements.

$$^{3*}\mathrm{F} + \mathrm{Q} \underset{k_{-\mathrm{d}}}{\overset{k_{\mathrm{d}}}{\rightleftharpoons}} \{^{3*}\mathrm{F}\cdots\mathrm{Q}\} \xrightarrow{k_{\mathrm{P}e\mathrm{T}}} {}^{3*}\{\mathrm{F}^{\bullet-}\cdots\mathrm{Q}^{\bullet+}\} \quad (5)$$

$$\log\left(k_{\mathrm{P}e\mathrm{T}}^{\mathrm{obs}}\right) = \log(k_{\mathrm{d}}) - \log\left(1 + \frac{k_{-\mathrm{d}}}{k_{\mathrm{P}e\mathrm{T}}}\right) \quad (6)$$

$$k_{\mathrm{P}e\mathrm{T}} = \kappa(r)\upsilon e^{-\frac{\Delta E_{\mathrm{P}e\mathrm{T}}^{\ddagger}}{RT}} \quad (7)$$

$$\log\left(k_{\mathrm{P}e\mathrm{T}}^{\mathrm{obs}}\right) = \log(k_{\mathrm{d}}) - \log\left(1 + Z\cdot e^{\frac{\Delta E_{\mathrm{P}e\mathrm{T}}^{\ddagger}}{RT}}\right) \quad (8)$$

$$Z = \frac{k_{-\mathrm{d}}}{\kappa(r)\upsilon} \quad (9)$$

The correlation between $k_{\mathrm{P}e\mathrm{T}}^{\mathrm{obs}}$ and the activation energies calculated for each of our 16 different combinations is shown in Fig. 2a. Consistent with the reaction evolving from activation to diffusion controlled as the value of $\Delta E_{\mathrm{P}e\mathrm{T}}^{\ddagger}$ drops, $k_{\mathrm{P}e\mathrm{T}}^{\mathrm{obs}}$ is seen to increase in a parabolic manner and ultimately plateau as it reaches the value for the rate constant of diffusion (k_{d}). Here, a break point around 0.4 eV signals the transition from an activation- to a diffusion-controlled reaction. Eqn (8) provides a single parameter (Z, eqn (9)) to fit the functional relationship between experimental $k_{\mathrm{P}e\mathrm{T}}^{\mathrm{obs}}$ and theoretical $\Delta E_{\mathrm{P}e\mathrm{T}}^{\ddagger}$. Compounds serving as TSQs are thus sought where the $\Delta E_{\mathrm{P}e\mathrm{T}}^{\ddagger}$ values – calculated for their electron transfer to photoexcited cyanine dyes in the excited triplet state – ensure diffusion controlled quenching rate constants.

Analysis of Fig. 2a additionally shines light on the behaviour recorded for TSQs with different cyanines. It thus illustrates that β-ME, a well-known photostabilizer used with Cy3 and Cy5, is ineffective when used in conjunction with the bridged cyanine forms, Cy3B or Cy5B, as there is a significant activation barrier to PeT. While the values of $k_{\mathrm{P}e\mathrm{T}}^{\mathrm{obs}}$ recorded with Cy3–βME and Cy5–βME are on the order of 10^8 M^{-1} s^{-1}, the values for Cy3B–βME and Cy5B–βME drop by one and two orders of magnitude to $\sim 10^7$ and 10^6 M^{-1} s^{-1}, respectively. Likewise, n-PG and AA show the same trend, where $k_{\mathrm{P}e\mathrm{T}}^{\mathrm{obs}}$ follows the order Cy3 > Cy5 > Cy3B > Cy5B. In the case of TX, Cy5 and Cy3B invert the order, rendering Cy3 > Cy3B > Cy5 > Cy5B. For TX and AA, the diffusion-controlled regime is reached with Cy3, although most of the pairs are in the activation energy-controlled regime. Although all dyes exhibit a diffusion-limited rate with n-PG, its low solubility, and the high likelihood of radicals in the triplet manifold escaping and reacting elsewhere, poses a significant drawback for its universal applicability.

Importantly, while the correlation of $k_{\mathrm{P}e\mathrm{T}}^{\mathrm{obs}}$ with $\Delta E_{\mathrm{P}e\mathrm{T}}^{\ddagger}$ provided satisfactory results, correlations with calculated values
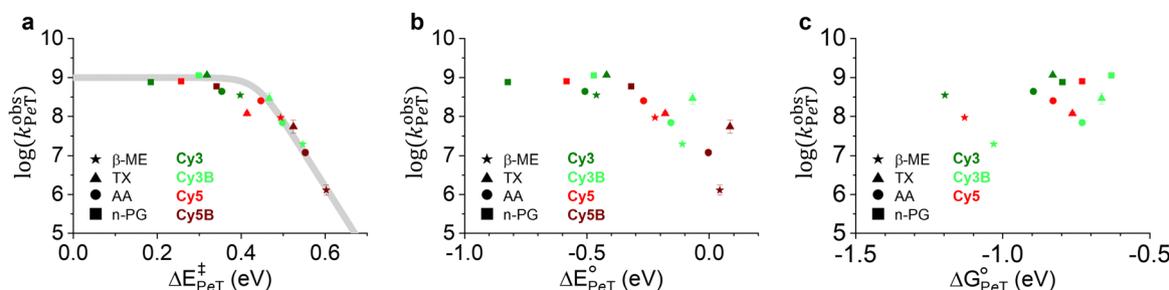

Fig. 2 Empirical PeT rate constant ($k_{\mathrm{P}e\mathrm{T}}^{\mathrm{obs}}$) as a function of different energy parameters: (a) the theoretical activation energy of the PeT process $\left(\Delta E_{\mathrm{P}e\mathrm{T}}^{\ddagger}\right)$ or (b) the theoretical free energy of the PeT process $\left(\Delta E_{\mathrm{P}e\mathrm{T}}^{\circ}\right)$ obtained via DFT modelling; and (c) the Gibbs free energy of the PeT process obtained from experimental redox potentials and triplet energies. TSQ–dye pairs are presented as a combination of icon and color, respectively. Panel (a) is fitted with eqn (8).

9230 | *Phys. Chem. Chem. Phys.*, 2025, **27**, 9227–9234

This journal is © the Owner Societies 2025

for the free energy change of the reaction ($\Delta E^{\circ}_{\text{P}e\text{T}}$, see the values in Table 1) or with experimental values of $\Delta G^{\circ}_{\text{P}e\text{T}}$ calculated through experimental values for their excited triplet state energy[35] and redox potentials (see Section S1.6, ESI,† for the experimental procedure and Table S4, ESI,† for values) yielded poorer outcomes (see Fig. 2b and c).

Screening and testing new thiol-based quenchers

We next set out to evaluate uncharted TSQ candidates with the developed computational model in hand. Here, the proposed theoretical-empirical strategy was used to screen thiol-containing compounds in search of superior TSQs (Fig. 3, data shown in Table S5, ESI†). The search for thiol-based electron-donors is rooted in the ability of the thiyl radical to undergo spin inversion, favoring the rapid triplet-to-singlet ISC of the newly formed geminate radical pair before solvent cage escape takes place. Initial candidates were identified that, based on our prediction, displayed diffusion-controlled PeT rate constants. Subsequent selection criteria were applied involving high solubility in water and low pK_a to ensure the thiolate is the dominant form at physiological pH. We also favored low vapor pressure compounds (reduced pungency).

Three targets were ultimately chosen utilizing our predictive model and selection criteria: ergothioneine (Erg), 2-thiol histidine (2-TH) and glyceryl monothioglycolate (GMTG). Erg and 2-TH were recently reported by our group as cyanine photostabilizers.[25] Consistent with our expectations, Erg exhibited diffusion-controlled values for $k^{\text{obs}}_{\text{P}e\text{T}}$ with Cy3, Cy3B, Cy5, and Cy5B and provided superior photoprotection for these cyanine dyes.

Turning the attention next to GMTG, this compound was selected based on its low pK_a (7.8),[26] low toxicity and its wide

range of predicted $k^{\text{obs}}_{\text{P}e\text{T}}$, facilitating the assessment of the model for a situation where a range of rate constants were predicted. The $k^{\text{obs}}_{\text{P}e\text{T}}$ values for GMTG with all four cyanines were determined experimentally using LFP. The experimentally obtained and predicted $k^{\text{obs}}_{\text{P}e\text{T}}$ values are summarized in Fig. 4a. The accurate prediction of $k^{\text{obs}}_{\text{P}e\text{T}}$ is apparent from the inspection in Fig. 4b, showing the linear correlation between the calculated (Calc.) and experimental (Exp.) $k^{\text{obs}}_{\text{P}e\text{T}}$ values obtained with GMTG, Erg, or 2-TH. Importantly, consistent with the previously reported rapid intersystem crossing observed within the geminate radical pair in the presence of newly formed thiyl radicals and leading to BeT before radical escape, transient absorption studies of Cy3B and Cy5B with GMTG showed negligible radical escape following PeT (Fig. S7, ESI†). The simultaneous decay of the excited triplet state and recovery of the ground state demonstrated efficient back electron transfer in the presence of GMTG as an electron donor, consistent with previous reports for β-ME[17] and ergothioneine.[25]

GMTG performance was then tested in single molecule fluorescence studies with Cy3 and Cy5 (Fig. 4c–f). While the predicted $k^{\text{obs}}_{\text{P}e\text{T}}$ rate constants for GMTG are smaller than those of β-ME, its pK_a is more than two units lower, indicating that GMTG should achieve a similar triplet quenching to that of β-ME with significantly lower total thiol concentrations. We thus tested GMTG in experiments conducted at three different concentrations: (1) a GMTG concentration that ensures the thiolate concentration is similar to that present when working with 143 mM β-ME, as estimated by their respective pK_a values; (2) a GMTG concentration that renders the same decay rate constant for the fluorophore excited triplet state (k_{T}) as that obtained with 143 mM of β-ME, and (3) a GMTG concentration that ensures a two-fold reduction of the triplet lifetime as
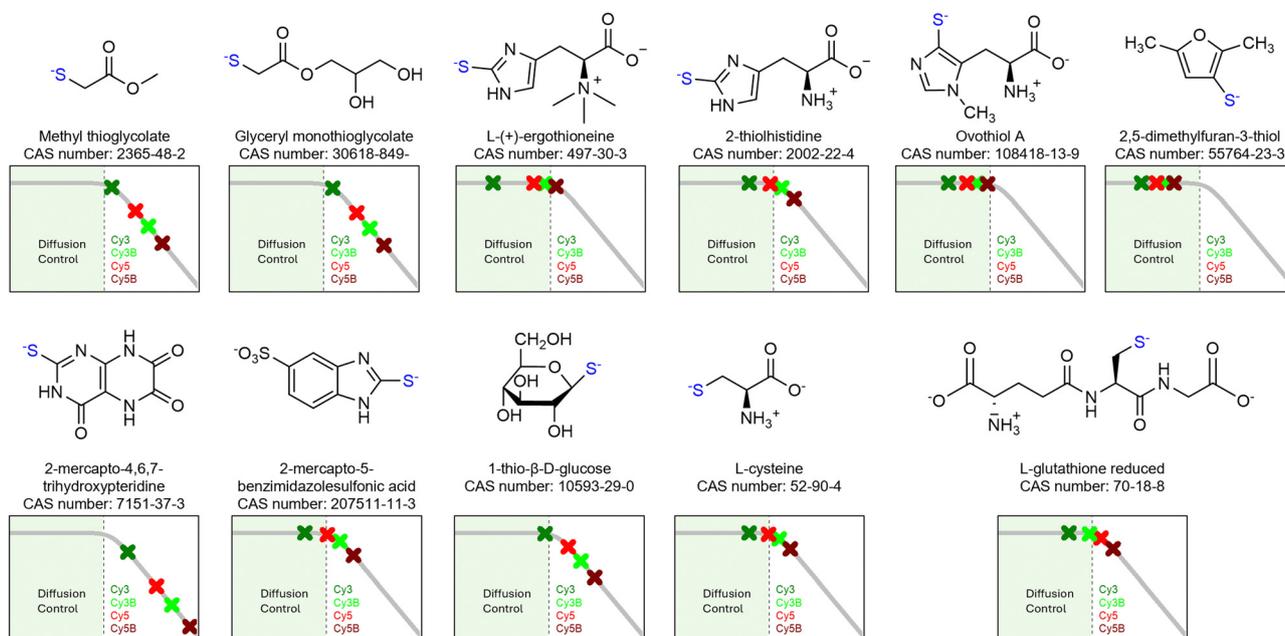

Fig. 3 Predicted $k^{\text{obs}}_{\text{P}e\text{T}}$ for thiolates with cyanine dyes. Molecules are parametrized as presented in their thiolate form. Rate constants are calculated after computing the DFT obtained energies, by using the fitting parameters obtained in the correlation model. Numerical data are presented in Table S5 (ESI†).

This journal is © the Owner Societies 2025

Phys. Chem. Chem. Phys., 2025, **27**, 9227–9234 | **9231**
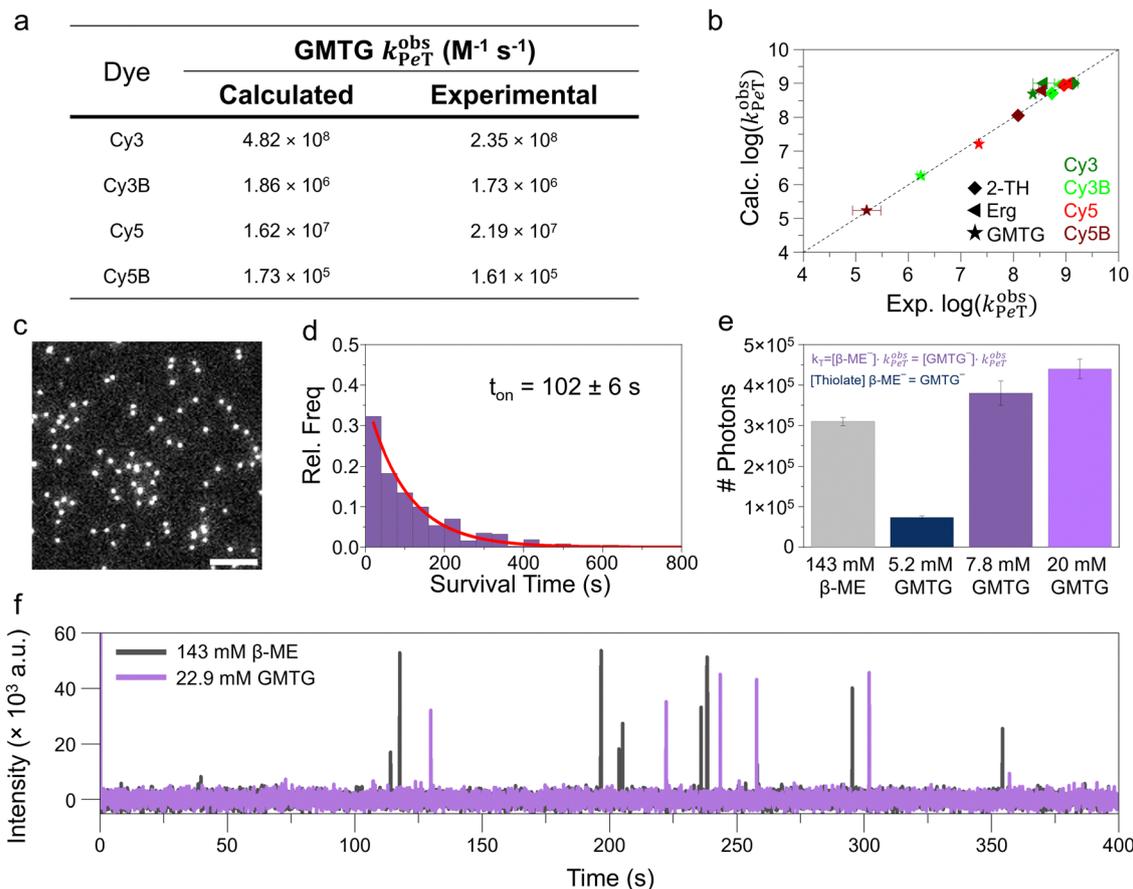
Fig. 4 (a) Calculated or experimentally determined k_{PeT}^{obs} for GMTG. (b) Calculated *versus* experimental $\log(k_{PeT}^{obs})$ values for GMTG, Erg and 2-TH to show the accuracy of the reported computational model. (c) Single molecule image of 7.8 mM GMTG with Cy3 (scale bar is 5 μm) and (d) the corresponding histogram for survival time (a marker of photostability). (e) Average number of total photons obtained in single molecule experiments of Cy3 with 143 mM β-ME and 5.2 mM GMTG yielding equal thiolate concentration as estimated by their respective pK_a values; at 7.8 mM GMTG ensuring equal quenching efficiency as that observed with 143 mM β-ME, and at an optimal GMTG concentration (20 mM); see Table S6 (ESI†). (f) Single molecule trajectories of Cy5 with 143 mM β-ME and 22.9 mM GMTG at 54 mW laser excitation power.

compared to β-ME. Cy3 and Cy5 were chosen based on their larger k_{PeT}^{obs}. Additionally, the former is expected to exhibit enhanced photostability, while the latter should display photo-induced blinking.

Single-molecule experiments were conducted with 18-mer single stranded DNA decorated with a single fluorophore dye and immobilized on the surface of a polyethylene glycol passivated glass coverslip.[36] The fluorophores were excited under standard total internal reflection microscopy conditions where images were captured with an EMCCD camera (Fig. 4c, see also Section S1.7, ESI,† for more information). The fluorescence response was recorded over time for the different GMTG concentrations. We extracted the total number of photons, survival time, and intensity per frame for each single molecule from the intensity-time trajectory. Data from all molecules were combined to create a probability distribution histogram (Fig. 4d). The obtained data exhibit an exponential decay, enabling determination of the average number of photons and survival time through fitting. These data were then compared with those from β-ME.

The average number of total photons obtained per fluorophore with 7.8 mM total GMTG ($\sim 3.8 \times 10^5$) was similar to that

recorded with 143 mM β-ME (Fig. 4e). Thus, a ~ 20-fold lower total GMTG concentration was required to achieve a comparable level of Cy3 photostabilization to that of β-ME, highlighting the potential of GMTG as an alternative to the latter. Improved results were obtained when increasing GMTG concentration by 2.56× (20 mM, see Fig. 4e). Here we note that with increasing GMTG concentration the intensity distribution shifted to smaller values (Fig. S8, ESI†). This shift can be attributed to partial quenching of the excited singlet states with increasing thiolate concentrations.

Single molecule studies with Cy5 in turn showed that GMTG leads to photoinduced blinking, as it has been shown for β-ME (Fig. 4f). As expected, given the precursor nature of the thiolate in forming the Cy5–thiol adduct,[12,17] both the duration of the dwell-on time and accordingly the number of photons per blink got reduced as we increase the GMTG concentration (Table S7, ESI†). Importantly the number of photons per blink (~ 2200 photons) and the intensity per unit time during a blink were similar regardless of the thiol source at comparable quenching rates (143 mM β-ME *vs.* 22.9 mM GMTG), highlighting the importance (an advantage) of a lower pK_a for thiol-based switching agents. Notably, the lifetime of the dark adduct under our experimental conditions

was one order of magnitude larger for GMTG than for β-ME, going from ∼11 s to ∼100 s for β-ME *vs.* GMTG, respectively. This discrepancy may reflect either a decrease in the extinction coefficient for the adduct, or in the acid catalyzed uncaging rate constant of the Cy5–GMTG adduct.[17] The increased lifetime for the dark adduct would enable better duty cycles and enhanced resolution in SMLM for GMTG when compared with β-ME.

Conclusions

We have developed an *in silico* strategy that allows us to predict P*e*T rate constants for potential excited triplet state quenchers of cyanine dyes. These compounds are a valuable resource in single-molecule fluorescence imaging to modulate the performance of fluorophores, *e.g.*, by retarding their fading, allowing extension of the visualization of the system under study with increased signal stability, or by entering into a photoswitching state, a key parameter for successful super-resolution studies.

Our model is a valuable tool for rapid computational testing of potentially effective triplet quenchers. This strategy can avoid a lengthy synthesis and further screening through single-molecule methods for promising molecules, a resource- and labor-intensive task. Since both the dye and the quencher are modeled separately, parameters described herein can be directly applied to combinations with new triplet state quenchers after calculations for the latter are performed. Our method should be directly extended to structurally related cyanine fluorophores. We also anticipate that this strategy, with proper calibration, can also be extended to other dyes utilized in single-molecule studies, *e.g.* rhodamines.

A series of thiol-based compounds were selected though our screening method, where a versatile thiol of ample use by the general public was singled out, due to its low vapor pressure and toxicity, and desirable solubility and acidity. While this work highlights the opportunities brought by this compound toward single molecule fluorescence imaging and super-resolution, most importantly, it underscores the potential of the model to rapidly screen for optimal photostabilizers using the vast number of available compounds. It is also relevant to mention that the model is certainly applicable to all scenarios where P*e*T is a desired outcome in the encounter between an excited organic chromophore and an electron donor/acceptor quencher. While this work emphasizes the need for back electron transfer toward photostabilization and photoswitching, and thus the choice of thiol-based compounds as P*e*T electron donors, certainly similar ideas could be extended in, *e.g.*, photoredox catalysis, where the desired outcome would be escape of newly formed transient species from a solvent cage, rather than back electron transfer.

Data availability

The following files are available in the ESI:† materials, computational methods and laser flash photolysis studies, electrochemical studies and single molecule fluorescence microscopy methodologies (PDF). DFT calculations are available in Figshare at https://doi.org/10.6084/m9.figshare.27996854.

Conflicts of interest

There are no conflicts to declare.

Acknowledgements

References

1 W. E. Moerner and D. P. Fromm, *Rev. Sci. Instrum.*, 2003, **74**, 3597–3619.

2 S. Samanta, K. Lai, F. Wu, Y. Liu, S. Cai, X. Yang, J. Qu and Z. Yang, *Chem. Soc. Rev.*, 2023, **52**, 7197–7261.

3 P. S. Dittrich and P. Schwille, *Appl. Phys. B: Lasers Opt.*, 2001, **73**, 829–837.

4 Y. Lin, J. J. Long, F. Huang, W. C. Duim, S. Kirschbaum, Y. Zhang, L. K. Schroeder, A. A. Rebane, M. G. Velasco, A. Virrueta, D. W. Moonan, J. Jiao, S. Y. Hernandez, Y. Zhang and J. Bewersdorf, *PLoS One*, 2015, **10**, e0128135.

5 A. P. Demchenko, *Methods Appl. Fluoresc.*, 2020, **8**, 022001.

6 R. Y. Tsien and A. Waggoner, in *Handbook of Biological Confocal Microscopy*, ed. J. B. Pawley, Springer, Boston, MA, 1995, ch 16, pp. 267–279, DOI: 10.1007/978-1-4757-5348-6_16.

7 M. J. Rust, M. Bates and X. Zhuang, *Nat. Methods*, 2006, **3**, 793–796.

8 M. Bates, T. R. Blosser and X. Zhuang, *Phys. Rev. Lett.*, 2005, **94**, 108101.

9 M. Lelek, M. T. Gyparaki, G. Beliu, F. Schueder, J. Griffie, S. Manley, R. Jungmann, M. Sauer, M. Lakadamyali and C. Zimmer, *Nat. Rev. Methods Primers*, 2021, **1**, 39.

10 L. Herdly, P. W. Tinning, A. Geiser, H. Taylor, G. W. Gould and S. van de Linde, *J. Phys. Chem. B*, 2023, **127**, 732–741.

11 L. A. Campos, J. Liu, X. Wang, R. Ramanathan, D. S. English and V. Muñoz, *Nat. Methods*, 2011, **8**, 143–146.

12 G. T. Dempsey, M. Bates, W. E. Kowtoniuk, D. R. Liu, R. Y. Tsien and X. Zhuang, *J. Am. Chem. Soc.*, 2009, **131**, 18192–18193.

This journal is © the Owner Societies 2025

Phys. Chem. Chem. Phys., 2025, **27**, 9227–9234 | 9233

13 T. Ha and P. Tinnefeld, *Annu. Rev. Phys. Chem.*, 2012, **63**, 595–617.

14 P. Eiring, R. McLaughlin, S. S. Matikonda, Z. Han, L. Grabenhorst, D. A. Helmerich, M. Meub, G. Beliu, M. Luciano, V. Bandi, N. Zijlstra, Z. D. Shi, S. G. Tarasov, R. Swenson, P. Tinnefeld, V. Glembockyte, T. Cordes, M. Sauer and M. J. Schnermann, *Angew. Chem., Int. Ed.*, 2021, **60**, 26685–26693.

15 J. Widengren, A. Chmyrov, C. Eggeling, P.-Å. Löfdahl and C. A. M. Seidel, *J. Phys. Chem. A*, 2007, **111**, 429–440.

16 P. Holzmeister, A. Gietl and P. Tinnefeld, *Angew. Chem., Int. Ed.*, 2014, **53**, 5685–5688.

17 Y. Gidi, L. Payne, V. Glembockyte, M. S. Michie, M. J. Schnermann and G. Cosa, *J. Am. Chem. Soc.*, 2020, **142**, 12681–12689.

18 V. Glembockyte and G. Cosa, *J. Am. Chem. Soc.*, 2017, **139**, 13227–13233.

19 M. S. Michie, R. Gotz, C. Franke, M. Bowler, N. Kumari, V. Magidson, M. Levitus, J. Loncarek, M. Sauer and M. J. Schnermann, *J. Am. Chem. Soc.*, 2017, **139**, 12406–12409.

20 T. Yanagida, M. Nakase, K. Nishiyama and F. Oosawa, *Nature*, 1984, **307**, 58–60.

21 J. Vogelsang, R. Kasper, C. Steinhauer, B. Person, M. Heilemann, M. Sauer and P. Tinnefeld, *Angew. Chem., Int. Ed.*, 2008, **47**, 5465–5469.

22 A. Longin, C. Souchier, M. Ffrench and P. A. Bryon, *J. Histochem. Cytochem.*, 1993, **41**, 1833–1840.

23 T. Cordes, J. Vogelsang and P. Tinnefeld, *J. Am. Chem. Soc.*, 2009, **131**, 5018–5019.

24 I. Rasnik, S. A. McKinney and T. Ha, *Nat. Methods*, 2006, **3**, 891–893.

25 Y. Gidi, J. Ramos-Sanchez, T. C. Lovell, V. Glembockyte, I. K. Cheah, M. J. Schnermann, B. Halliwell and G. Cosa, *J. Am. Chem. Soc.*, 2023, **145**, 19571–19577.

26 C. Bouillon and J. Wilkinson, *The Science of hair care*, Taylor & Francis Group, LLC, Boca Raton, Florida, 2nd edn, 2005.

27 R. A. Marcus and N. Sutin, *Biochim. Biophys. Acta, Bioenerg.*, 1985, **811**, 265–322.

28 J. W. Ochterski, *Thermochemistry in Gaussian*, 2000.

29 M. J. Frisch, G. W. Trucks, H. B. Schlegel, G. E. Scuseria, M. A. Robb, J. R. Cheeseman, G. Scalmani, V. Barone, G. A. Petersson, H. Nakatsuji, X. Li, M. Caricato, A. V. Marenich, J. Bloino, B. G. Janesko, R. Gomperts, B. Mennucci, H. P. Hratchian, J. V. Ortiz, A. F. Izmaylov, J. L. Sonnenberg, D. Williams-Young, F. Ding, F. Lipparini, F. Egidi, J. Goings, B. Peng, A. Petrone, T. Henderson, D. Ranasinghe, V. G. Zakrzewski, J. Gao, N. Rega, G. Zheng, W. Liang, M. Hada, M. Ehara, K. Toyota, R. Fukuda, J. Hasegawa, M. Ishida, T. Nakajima, Y. Honda, O. Kitao, H. Nakai, T. Vreven, K. Throssell, J. A. Montgomery, Jr., J. E. Peralta, F. Ogliaro, M. J. Bearpark, J. J. Heyd, E. N. Brothers, K. N. Kudin, V. N. Staroverov, T. A. Keith, R. Kobayashi, J. Normand, K. Raghavachari, A. P. Rendell, J. C. Burant, S. S. Iyengar, J. Tomasi, M. Cossi, J. M. Millam, M. Klene, C. Adamo, R. Cammi, J. W. Ochterski, R. L. Martin, K. Morokuma, O. Farkas, J. B. Foresman and D. J. Fox, *Gaussian 16, Revision A.03*, Gaussian, Inc., Wallingford CT, 2016.

30 M. Buda, *Electrochim. Acta*, 2013, **113**, 536–549.

31 B. Sauerwein and G. B. Schuster, *J. Phys. Chem.*, 1991, **95**, 1903–1906.

32 K. Jia, Y. Wan, A. Xia, S. Li, F. Gong and G. Yang, *J. Phys. Chem. A*, 2007, **111**, 1593–1597.

33 R. E. Benesch and R. Benesch, *Science*, 1953, **118**, 447–448.

34 D. Rehm and A. Weller, *Isr. J. Chem.*, 1970, **8**, 259–271.

35 Q. Zheng, S. Jockusch, G. G. Rodriguez-Calero, Z. Zhou, H. Zhao, R. B. Altman, H. D. Abruna and S. C. Blanchard, *Photochem. Photobiol. Sci.*, 2016, **15**, 196–203.

36 Y. Gidi, S. Bayram, C. J. Ablenas, A. S. Blum and G. Cosa, *ACS Appl. Mater. Interfaces*, 2018, **10**, 39505–39511.

9234 | *Phys. Chem. Chem. Phys.*, 2025, **27**, 9227–9234

This journal is © the Owner Societies 2025